Progress In Electromagnetics Research B, Vol. 43, 255–277, 2012

GENERAL 2-D TRANSIENT EDDY CURRENT FORCE EQUATIONS FOR A MAGNETIC SOURCE MOVING ABOVE A CONDUCTIVE PLATE

N. Paudel, S. Paul, and J. Z. Bird*

Department of Electrical and Computer Engineering, University of North Carolina at Charlotte, 9201 University City Boulevard, Charlotte, NC 29223, USA

Abstract—When a magnetic source is moved and/or oscillating above a conductive linear plate a traveling time varying magnetic field is created in the airgap. This field induces eddy currents in the plate that can simultaneously create normal and tangential forces. The transient fields and the forces created by the magnetic source are modeled using a novel 2-D analytic based **A**-ϕ method in which the presence of the source field is incorporated into the boundary conditions of the plate. The analytic based solution is obtained by using the spatial Fourier transform and temporal Laplace transform. The performance of the method is compared with a 2-D transient finite element model with a Halbach rotor source field. The derived transient force equations are written in a general form so that they can be applied to any magnetic source.

1. INTRODUCTION

There are a large number of papers in which the steady-state force equations due to eddy currents in a linear conducting plate have been derived [1–8]. However, very few authors have derived exact analytic equations for transient eddy current forces. A number of authors have used the thin-sheet approximation method to compute the transient eddy current force response when translationally moving a current filament above a conducting sheet [9–12]. However the thin-sheet approximation assumes that the current distribution is constant throughout the track thickness and this is not the case under almost any transient condition and has been shown to be inaccurate when there is a steady-state oscillating and translationally moving field [13].

Received 24 July 2012, Accepted 20 August 2012, Scheduled 6 September 2012

* Corresponding author: Jonathan Z. Bird (j.bird@uncc.edu).

Langerholc derived transient force equations for a vertically perturbed coil without the thin-sheet approximation. However, the forces were computed by using the reflected field due to the eddy currents onto the source coil [14] and therefore the derivation is source dependent which makes it difficult to directly apply to problems involving complicated magnetic sources. In this paper, the transient forces are computed on the surface of the conducting plate. The advantage of this approach is that forces due to a complicated source, such as the Halbach rotor shown in Figure 1 [15] can be determined with relative ease since the force integral only needs to be applied along the surface of the conducting plate.

Numerical based transient eddy current methods based on the finite element method (FEA) [16, 17] and boundary element method [18] are readily available. However when trying to develop advanced control strategies the numerical based software must be coupled into other programs such as Matlab and/or Simulink and this can lead to extremely long simulation times [19]. Therefore, analytic based transient eddy current force models can be particularly useful when trying to develop real-time transient based electromechanical control strategies.

In this paper, the transient response due to a sudden change in the source field will be derived under the assumption that the forces are initially in a steady-state condition. The conducting region is formulated in terms of the magnetic vector potential, A_z, and the non-conducting regions are formulated in terms of the magnetic scalar potential, ϕ. The force is computed on the conducting boundary using the Maxwell stress tensor method. The force equations are derived

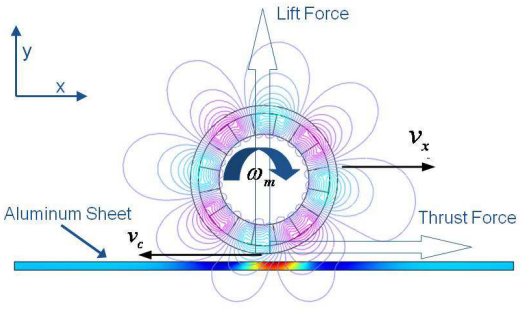

Figure 1. Plot from a finite element analysis COMSOL model for a 4 pole-pair Halbach rotor rotating and translationally moving above an aluminum plate. The field created by the Halbach rotor is shown as well as the induced currents within the aluminum conductive plate.

in a general way so that any magnetic or current source can be used. It is shown that the force equations can be greatly simplified if the transmitted field is written in terms of the source and reflected field on the conductor plate boundary [20]. The force equations are validated by verifying them with a transient model of a Halbach rotor that is both rotating and translationally moving above a conductive plate as illustrated in Figure 1. The Halbach rotor is assumed to be very long and the conductor plate width is assumed to be significantly greater than the source width.

The results present in this paper will be useful for gaining a deeper understanding of the transient effects encountered in eddy current damping [21], braking [22], and maglev transportation [19, 23, 24] as well as for Lorentz force eddy current non-destructive testing [25] applications.

2. GOVERNING EQUATIONS

2.1. Conducting Plate Region, Ω_2

The 2-D governing equation in the linear conductive region is

$$\frac{\partial^2 A_z}{\partial x^2} + \frac{\partial^2 A_z}{\partial y^2} = \mu_0 \sigma \frac{\partial A_z}{\partial t} \tag{1}$$

2.2. Non-conducting Regions, Ω_1, Ω_3

Within the non-conducting regions, with a source field present, the total magnetic flux density, $\mathbf{B}$, can be expressed as the sum of a source field

$$\mathbf{B}^s = B_x^s(x, y, t)\hat{\mathbf{x}} + B_y^s(x, y, t)\hat{\mathbf{y}} \tag{2}$$

and a reflected flux density $\mathbf{B}^r$ due to induced eddy currents, such that

$$\mathbf{B}(x, y, t) = \mathbf{B}^s(x, y, t) + \mathbf{B}^r(x, y, t) \tag{3}$$

The reflected field can be further written in terms of the scalar potential, ϕ_n, defined as

$$\mathbf{B}^r = -\mu_0 \nabla \phi_n \quad \text{in } \Omega_n. \tag{4}$$

where $n = 1$, 3 for region 1 and 3 respectively. After taking the divergence of both sides of (3) the formulation in the non-conducting region will reduce to

$$\frac{\partial^2 \phi_n}{\partial x^2} + \frac{\partial^2 \phi_n}{\partial y^2} = 0 \quad \text{in } \Omega_n. \tag{5}$$

Therefore, as $\nabla \cdot \mathbf{B}^s = 0$ it is not necessary to model the source within the non-conducting region [26]. The source field will show up only on the conductive boundary. The model for the analytic based solution is shown in Figure 2 and is composed of a conducting region Ω_2 and two non-conducting regions Ω_1, Ω_3.

2.3. Boundary Conditions

The boundary interface conditions for the tangential and normal field components along the Γ_{12} interface can be expressed in terms of a reflected, transmitted and source field. This is illustrated in Figure 3. The x-component of the reflected, B_x^r, and transmitted, B_x^t, eddy current flux density components are related by

$$B_x^t(x,b,t) = B_x^s(x,b,t) + B_x^r(x,b,t) \quad \text{on } \Gamma_{12} \tag{6}$$

Similarly, the y-component reflected B_y^r and transmitted, B_y^t flux density components are related by

$$B_y^t(x,b,t) = B_y^s(x,b,t) + B_y^r(x,b,t) \quad \text{on } \Gamma_{12} \tag{7}$$

In terms of magnetic vector, A_z and scalar ϕ_1 (6) and (7) are [8]

$$\frac{\partial A_z(x,y,t)}{\partial y}\bigg|_{y=b} = B_x^s(x,b,t) - \mu_0 \frac{\partial \phi_1(x,b)}{\partial x} \quad \text{on } \Gamma_{12} \tag{8}$$

$$-\frac{\partial A_z(x,b,t)}{\partial x} = B_y^s(x,b,t) - \mu_0 \frac{\partial \phi_1(x,y)}{\partial y}\bigg|_{y=b} \quad \text{on } \Gamma_{12} \tag{9}$$

The source is located only in region Ω_1 therefore the boundary conditions on Γ_{23} are

$$-\mu_0 \frac{\partial \phi_3(x,0)}{\partial x} = \frac{\partial A_z(x,y,t)}{\partial y}\bigg|_{y=0} \quad \text{on } \Gamma_{23} \tag{10}$$

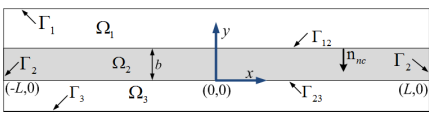

Figure 2. Illustration of the conductive (Ω_2) and non-conductive (Ω_1, Ω_3) regions and boundaries used by the analytic based model.

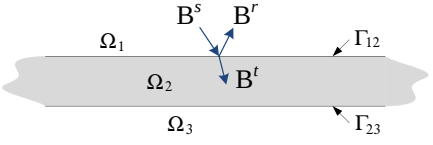

Figure 3. Separation of the eddy current fields into reflected and transmitted fields can greatly reduce the computational complexity.

$$-\mu_0 \left.\frac{\partial \phi_3(x,y)}{\partial y}\right|_{y=0} = -\frac{\partial A_z(x,0,t)}{\partial x} \quad \text{on } \Gamma_{23} \tag{11}$$

The source field is assumed to be centrally located at $x = 0$ and the plate is sufficiently long to ensure that the field is zero at the conductive plate ends ($x = \pm L$)

$$B_x^s(\pm L, y, t) = 0, \quad \text{on } \Gamma_2 \tag{12}$$

$$B_y^s(\pm L, y, t) = 0, \quad \text{on } \Gamma_2 \tag{13}$$

$$A_z(\pm L, y, t) = 0, \quad \text{on } \Gamma_2 \tag{14}$$

Also, on the outer non-conducting boundaries, one has

$$\phi_1 = 0, \quad \text{on } \Gamma_1 \tag{15}$$

$$\phi_2 = 0, \quad \text{on } \Gamma_3 \tag{16}$$

2.4. Source Field

In this paper, the source field is assumed to be created by a 2-D Halbach rotor which can simultaneously rotate and translationally move. The analytic solution for the 2-D Halbach rotor was derived in [27]. In terms of the vector potential it is given by [8]

$$A_z^s(r,\theta) = \frac{C}{P}\frac{e^{j(\omega_{e1}t + P\theta)}}{r^P} \tag{17}$$

where

$$C = \left(\frac{2B_r P}{P+1}\right)\frac{(1+\mu_r)r_o^{2P}\left(r_o^{P+1} - r_i^{P+1}\right)}{(1-\mu_r)^2 r_i^{2P} - (1+\mu_r)^2 r_o^{2P}} \tag{18}$$

B_r = magnet residual flux density, μ_r = relative permeability, r_o = outer rotor radius, r_i = inner rotor radius, P = rotor pole-pairs and ω_{e1} = rotor angular electrical velocity. The rotor angular velocity is related to the mechanical angular velocity by $\omega_{e1} = \omega_m P$. The magnet eddy current losses are neglected in the analysis but as the Halbach magnets are highly segmented, these losses will be relatively low [28]. Recalling from complex analysis that

$$\frac{1}{x - jy} = \frac{e^{j\theta}}{r} \tag{19}$$

where $r = (x^2 + y^2)^{1/2}$; then by comparing (17) with (19) one can express (17) in Cartesian coordinates

$$A_z^s(x,y) = \frac{Ce^{j\omega_{e1}t}}{P(x - jy)^P} \tag{20}$$

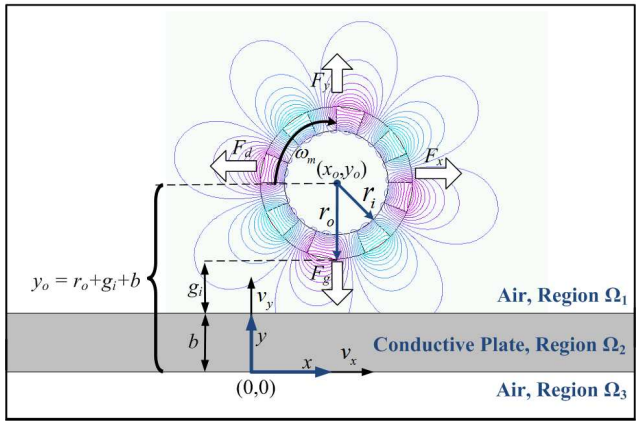

Figure 4. Halbach rotor source fields with y-axis offset.

The rotor magnetic flux density components for a four pole-pair, $P = 4$, rotor are then given by

$$B_x^s(x,y) = \frac{\partial A_z^s}{\partial y} = \frac{jC}{(x-jy)^5} e^{j\omega_{e1}t} \tag{21}$$

$$B_y^s(x,y) = -\frac{\partial A_z^s}{\partial x} = \frac{C}{(x-jy)^5} e^{j\omega_{e1}t} \tag{22}$$

The rotor field derivation above assumes that the rotor is centered at $(x,y) = (0,0)$. While the conductive plate problem has $(x,y) = (0,0)$ at the base of the plate. This is shown in Figure 4. Therefore, a y coordinate offset is required, including this offset (22) and (21) can be written as

$$B_y^s(x,y) = \frac{C}{(x-v_{x1}t-j(y-y_o))^5} e^{j\omega_{e1}t} \tag{23}$$

$$B_x^s(x,y) = jB_y^s(x,y) \tag{24}$$

where $y_o = r_o + g_i + b$ is defined as the distance from the center of the rotor to the bottom of the conductive plate, and g_i is the air-gap distance between the rotor surface and the conducting plate. In addition, a translational velocity, v_{x1}, has been added into (23) and (24).

3. FOURIER-LAPLACE ANALYTIC SOLUTION

The governing equations for the problem regions are given by (1) and (5). These equations must satisfy the boundary conditions (8)–(16). The transient solution to this problem has been obtained by

using the spatial Fourier transform on x defined as

$$A_z(\xi, y, t) = \int_{-\infty}^{\infty} A_z(x, y, t) e^{-j\xi x} dx \tag{25}$$

$$\phi_n(\xi, y) = \int_{-\infty}^{\infty} \phi_n(x, y) e^{-j\xi x} d\xi \tag{26}$$

and the Laplace transform on time, t, which is defined as

$$A_z(\xi, y, s) = \int_{0}^{\infty} A_z(\xi, y, t) e^{-st} dt \tag{27}$$

3.1. Fourier and Laplace Transformed Problem Regions

By utilizing (25) the Fourier transform of (1) for the conducting region is

$$\frac{\partial^2 A_z(\xi, y, t)}{\partial y^2} = \mu_0 \sigma \frac{\partial A_z(\xi, y, t)}{\partial t} + \xi^2 A_z(\xi, y, t) \tag{28}$$

Using the definition of the temporal Laplace transform, (27), (28) reduces down to

$$\frac{\partial^2 A_z(\xi, y, s)}{\partial y^2} = \gamma^2 A_z(\xi, y, s) - \mu_0 \sigma A_z^{ss}(\xi, y, t_0) \tag{29}$$

where

$$\gamma^2 = \xi^2 + \mu_0 \sigma s \tag{30}$$

and $A_z^{ss}(\xi, y, t_0)$ is an initial steady-state solution within the conductive region at an initial time t_0. This steady-state vector potential solution for a source field operating at frequency ω_{e0} and moving with velocity v_{x0} above a conductive plate is given by [8]

$$A_z^{ss}(\xi, y, t_0) = T(\xi, y, s_0) B^{s0}(\xi, b) e^{j\omega_{e0} t_0} \tag{31}$$

$T(\xi, y, s)$ is the transmission function defined as

$$T(\xi, y, s) = \frac{(\gamma + \xi) e^{\gamma y} + (\gamma - \xi) e^{-\gamma y}}{e^{\gamma b} (\gamma + \xi)^2 - e^{-\gamma b} (\gamma - \xi)^2} \tag{32}$$

and

$$s_0 = j\omega_{e0} + v_{x0}\xi \tag{33}$$

$$B^{s0}(\xi, b) = B_x^{s0}(\xi, b) + jB_y^{s0}(\xi, b) \tag{34}$$

The solution to (29) is given by

$$A_z(\xi, y, s) = \frac{A_z^{ss}(\xi, y, t_0)}{s - s_0} + M(\xi, s)e^{y\gamma} + N(\xi, s)e^{-y\gamma} \tag{35}$$

where the unknowns $M(\xi, s)$ and $N(\xi, s)$ need to be determined. Fourier transforming the non-conducting region governing equation, (5), yields

$$\frac{\partial^2 \phi_n(\xi, y)}{\partial y^2} = \xi^2 \phi_n(\xi, y) \quad \text{in } \Omega_n \tag{36}$$

where $n = 1$ and 3. Solving (36) and noting that when moving away from the conductive plate along the y-axis in Ω_1 and Ω_3 the field must reduce to zero, one obtains the solutions

$$\phi_1(\xi, y, s) = X_1(\xi, s)e^{-\xi y} \quad \text{in } \Omega_1 \tag{37}$$

$$\phi_3(\xi, y, s) = X_3(\xi, s)e^{\xi y} \quad \text{in } \Omega_3 \tag{38}$$

The changing field with respect to time external to the conducting plate depends on the X_1 and X_3 terms.

3.2. Fourier and Laplace Transformed Boundary Conditions

Fourier and Laplace transforming the top conducting boundary condition given by (8) and (9) one obtains

$$-j\mu_0 \xi \phi_1(\xi, b, s) + B_x^s(\xi, b, s) = \left.\frac{\partial A_z(\xi, y, s)}{\partial y}\right|_{y=b} \quad \text{on } \Gamma_{12} \tag{39}$$

$$-\mu_0 \left.\frac{\partial \phi_1(\xi, y, s)}{\partial y}\right|_{y=b} + B_y^s(\xi, b, s) = -j\xi A_z(\xi, b, s) \quad \text{on } \Gamma_{12} \tag{40}$$

Substituting the vector and scalar potential solution (35), (37) into (39), (40) and eliminating ϕ_1 yields

$$B^{s1}(\xi, b, s) = \frac{B^{ss}(\xi, b, t_0)}{s - s_0} + (\xi + \gamma)M(\xi, s)e^{b\gamma} + (\xi - \gamma)N(\xi, s)e^{-b\gamma} \tag{41}$$

where

$$B^{ss}(\xi, b, t_0) = \frac{\partial A_z^{ss}(\xi, y, t_0)}{\partial y} + \xi A_z^{ss}(\xi, y, t_0) \tag{42}$$

$$B^s(\xi, b, s) = B_x^s(\xi, b, s) + jB_y^s(\xi, b, s) \tag{43}$$

Equation (43) is a complex scalar term and not the vector term defined by (2). Evaluating (42) it is determined that

$$B^{ss}(\xi, b, t_0) = B^{s0}(\xi, b)e^{j\omega_{e0}t_0} \tag{44}$$

where $B^{s0}(\xi, b)$ was defined by (34). The Fourier transform for the bottom boundary conditions (10)–(11) is

$$-j\mu_0\xi\phi_3(\xi, 0, s) = \left.\frac{\partial A_z(\xi, y, s)}{\partial y}\right|_{y=0}, \quad \text{on } \Gamma_{23} \tag{45}$$

$$-\mu_0 \left.\frac{\partial \phi_3(\xi, y, s)}{\partial y}\right|_{y=0} = -j\xi A_z(\xi, 0, s), \quad \text{on } \Gamma_{23} \tag{46}$$

substituting the value of vector and scalar potential solution, (38), into (45), (46) and eliminating ϕ_3 gives

$$M(\xi, s) = N(\xi, s)\frac{\xi + \gamma}{\gamma - \xi} \tag{47}$$

3.3. The Solution of the Governing Equation

Substituting (47) and (44) into (41) one obtains

$$N(\xi, s) = \frac{(\gamma - \xi)\left[B^{s1}(\xi, b, s)(s - s_0) - B^{s0}(\xi, b)e^{j\omega_{e0}t_0}\right]}{(s - s_0)\left[e^{\gamma b}(\gamma + \xi)^2 - e^{-\gamma b}(\gamma - \xi)^2\right]} \tag{48}$$

Substituting (47) and (48) into (35) gives

$$A_z(\xi, y, s) = T(\xi, y, s)\left[B^{s1}(\xi, b, s) - \frac{B^{s0}(\xi, b)e^{j\omega_{e0}t_0}}{(s - s_0)}\right] + \frac{A_z^{ss}(\xi, y, t_0)}{s - s_0} \tag{49}$$

The second term in (49) is the steady-state solution and the first term is the transient solution due to the change in source field. If the new value of the source field in the time domain is assumed to be

$$B^{s1}(\xi, b, t) = B^{s1}(\xi, b)e^{s_1 t} \tag{50}$$

where

$$s_1 = j(\omega_{e1} + v_{x1}\xi) \tag{51}$$

Then after Laplace transforming (50) the solution (49) can be written as

$$A_z(\xi, y, s) = \left[\frac{B^{s1}(\xi, b)}{s - s_1} - \frac{B^{s0}(\xi, b)e^{j\omega_{e0}t_0}}{s - s_0}\right] T(\xi, y, s) + \frac{A_z^{ss}(\xi, y, t_0)}{s - s_0} \tag{52}$$

The translational motion of the magnetic source has been accounted for by moving the magnetic source. While the steady-state model accounts for the motion of the source by including the velocity term within the transmission function. Either approach is possible when modeling the problem transiently [29].

3.4. Reflected and Transmitted Flux Density in Ω_1

The reflected eddy current field can be determined by solving for $X_1(\xi)$ in Ω_1. Substituting (37) into (40) and rearranging gives

$$X_1(\xi, s) = \frac{-1}{\mu_0 \xi} \left[j\xi A_z(\xi, b, s) + B_y^s(\xi, b, s) \right] e^{\xi b} \tag{53}$$

Substituting (53) into (37) one obtains

$$\phi_1(\xi, y, s) = \frac{-1}{\mu_0 \xi} \left[j\xi A_z(\xi, b, s) + B_y^s(\xi, b, s) \right] e^{\xi(b-y)} \tag{54}$$

From (54) it can be noted that the reflected flux density values B_x^r and B_y^r are given by

$$B_x^r(\xi, y, s) = j \left[j\xi A_z(\xi, b, s) + B_y^s(\xi, b, s) \right] e^{\xi(b-y)} \tag{55}$$

$$B_y^r(\xi, y, s) = - \left[j\xi A_z(\xi, b, s) + B_y^s(\xi, b, s) \right] e^{\xi(b-y)} \tag{56}$$

Thus, the reflected flux density components are related in Ω_1 by

$$B_y^r(\xi, y, s) = jB_x^r(\xi, y, s) \tag{57}$$

The transient reflected fields at $y = b$ is obtain by taking the inverse Laplace transform of (55) and (56)

$$B_x^r(\xi, b, t) = j \left[j\xi A_z(\xi, b, t) + B_y^s(\xi, b, t) \right] \tag{58}$$

$$B_y^r(\xi, b, t) = - \left[j\xi A_z(\xi, b, t) + B_y^s(\xi, b, t) \right] \tag{59}$$

where the transient vector potential $A_z(\xi, b, t)$ is derived in Section 5.

3.5. Source Field

The Fourier transform for the source field (23) and (24) is evaluated on the top conductor surface, $y = b$, this yields

$$B_x^s(\xi, b, t) = \frac{\pi}{12} C\xi^4 e^{-(r_o + g_1)\xi} e^{j(\omega_{e1} - \xi v_{x1})t} u(\xi) \tag{60}$$

$$B_y^s(\xi, b, t) = -jB_x^s(\xi, b, t) \tag{61}$$

where $u(\xi)$ is the step function [30]. Laplace transforming (60) and (61) gives

$$B_x^s(\xi, y, s) = \frac{1}{2} \frac{B^{s1}(\xi, b)}{s - s_1} \tag{62}$$

where

$$B_y^s(\xi, y, s) = -jB_x^s(\xi, y, s) \tag{63}$$

$$B^{s1}(\xi, b) = \frac{\pi}{6} C\xi^4 e^{-(r_o + g_1)\xi} u(\xi) \tag{64}$$

The steady-state source function at initial time $t = t_0$ used in (31) is given as

$$B^{s0}(\xi, b, t_0) = \frac{\pi}{6} C\xi^4 e^{-(r_o+g_0)\xi} u(\xi) e^{-j\omega_o t_o} \tag{65}$$

4. FORCE AND POWER LOSS

The tangential force, F_x, and normal force, F_y, can be determined by evaluating the stress tensor equations along the conductor surface ($y = b$). Due to Parseval's theorem this integration can be evaluated in the Fourier domain thereby avoiding the need to first obtain the inverse Fourier transform [6, 31]. The tangential and normal force equations are

$$F_x = \frac{w}{4\pi\mu_0} \mathrm{Re} \int_{-\infty}^{\infty} B_x^t B_y^{t*} d\xi \quad \text{on } \Gamma_{12} \tag{66}$$

$$F_y = \frac{w}{8\pi\mu_0} \mathrm{Re} \int_{-\infty}^{\infty} \left[B_y^t B_y^{t*} - B_x^t B_x^{t*} \right] d\xi \quad \text{on } \Gamma_{12} \tag{67}$$

the star superscript denotes complex conjugation and w is the width of the problem (into the page). The force equations can be greatly simplified if they are written in terms of the reflected and source fields.

4.1. Tangential and Normal Force, F_x, F_y

By substituting (6) and (7) into (66) the tangential force can be written in terms of the source and reflected field

$$F_x = \frac{w}{4\pi\mu_0} \mathrm{Re} \int_{-\infty}^{\infty} \left[B_x^r B_y^{s*} + B_x^s B_y^{r*} + B_x^s B_y^{s*} + B_x^r B_y^{r*} \right] d\xi \tag{68}$$

Substituting (57) into (68) and noting that

$$\mathrm{Re}\left[B_x^s B_y^{r*} \right] = \mathrm{Re}\left[B_y^r B_x^{s*} \right] \tag{69}$$

gives

$$F_x = \frac{w}{4\pi\mu_0} \mathrm{Re} \int_{-\infty}^{\infty} \left[B_y^r (B_x^{s*} - jB_y^{s*}) + B_x^s B_y^{s*} - j|B_x^r|^2 \right] d\xi \tag{70}$$

it can be noted that the real part of last term is zero. Substituting (59) into (70) and using the fact that

$$\mathrm{Re}[B_y^s B_x^{s*}] = \mathrm{Re}[B_y^{s*} B_x^s] \tag{71}$$

$$\mathrm{Re}[jB_y^s B_y^{s*}] = 0 \tag{72}$$

enables (68) to reduce down to

$$F_x = -\frac{w}{4\pi\mu_0}\mathrm{Re}\int_{-\infty}^{\infty}[j\xi A_z B^{s*}d\xi], \quad \text{on } \Gamma_{12} \tag{73}$$

Substituting (6) and (7) into (67) and rearranging gives

$$F_y = \frac{w}{8\pi\mu_0}\mathrm{Re}\int_{-\infty}^{\infty}\left[B_y^{s*}B_y^r + B_y^{r*}B_y^s - B_x^{s*}B_x^r - B_x^{r*}B_x^s + |B_y^s|^2 + |B_y^r|^2 - |B_x^s|^2 - |B_x^r|^2\right]d\xi, \quad \text{on } \Gamma_{12} \tag{74}$$

Using the relation (57) it can be noted that

$$\mathrm{Re}[|B_y^r|^2] = \mathrm{Re}[|B_x^r|^2] \tag{75}$$

$$\mathrm{Re}[B_y^{s*}B_y^r] = \mathrm{Re}[B_y^s B_y^{r*}] \tag{76}$$

$$\mathrm{Re}[B_x^{s*}B_x^r] = \mathrm{Re}[B_x^s B_x^{r*}] \tag{77}$$

utilizing these relationships (74) can be written as

$$F_y = \frac{w}{8\pi\mu_0}\mathrm{Re}\int_{-\infty}^{\infty}\left[-2B_x^r(B_x^{s*} - jB_y^{s*}) + |B_y^s|^2 - |B_x^s|^2\right]d\xi \tag{78}$$

Substituting (58) into (78) and rearranging yields

$$F_y = \frac{w}{8\pi\mu_0}\mathrm{Re}\int_{-\infty}^{\infty}\left[2\xi A_z B^{s*} - j2B_y^s B_x^{s*} - |B_y^s|^2 - |B_x^s|^2\right]d\xi \tag{79}$$

Noting that as B_y^s and B_x^s are complex the following is true

$$\mathrm{Re}\left[j2B_y^s B_x^{s*} + |B_y^s|^2 + |B_x^s|^2\right] = |B^s|^2 \tag{80}$$

Using (80) allows the normal force to be written as

$$F_y = \frac{w}{8\pi\mu_0}\mathrm{Re}\int_{-\infty}^{\infty}\left[2\xi A_z B^{s*} - |B^s|^2\right]d\xi, \quad \text{on } \Gamma_{12} \tag{81}$$

By comparing (73) with (81) it can be concluded that both the normal and tangential force can be calculated from the single integral

$$F(t) = \frac{w}{8\pi\mu_0}\int_{-\infty}^{\infty}\left[2\xi A_z(\xi,b,t)B^{s*}(\xi,b,t) - |B^s(\xi,b,t)|^2\right]d\xi, \text{ on } \Gamma_{12} \tag{82}$$

such that the normal and tangential force will be

$$F_y(t) = \mathrm{Re}[F(t)] \tag{83}$$

$$F_x(t) = \mathrm{Im}[F(t)] \tag{84}$$

This eliminates the need to evaluate separate force equations thus reducing the calculation time by half.

4.2. Power Loss, P_{Loss}

The work done per unit time, per unit volume is given by [32]

$$\frac{dW}{dt} = -\int_{\Gamma_{12}} \mathbf{S} \cdot d\Gamma_{12} - \frac{dU_{em}}{dt} \tag{85}$$

where $\mathbf{S}$ is the Poynting vector

$$\mathbf{S} = \mathbf{E} \times \mathbf{B} \tag{86}$$

and U_{em} is the total magnetic energy stored in the conductor region

$$U_{em} = \int_{\Omega} \frac{1}{2} \frac{\mathbf{B}^2}{\mu_0} d\Omega \tag{87}$$

In [8] the steady-state power transferred through the conductive plate was computing by evaluating the Poynting vector along Γ_{12}. However, the same method is not possible for the transient case because the total energy stored in the system which is given by the first term on the right side of (86) is not constant during the transient condition. In 2-D the transient power loss in the conducting plate can be more directly evaluated by using integral over the conduction plate surface

$$P_{loss}(t) = \frac{w}{4\pi\sigma} \int_{-\infty}^{\infty} \int_{0}^{b} \mathrm{Re}\left[J_z(x,y,t) J_z^*(x,y,t)\right] d\Omega \tag{88}$$

Using Parseval's theorem the power loss can be directly evaluated in the Fourier domain

$$P_{loss} = \frac{w}{4\pi\sigma} \int_{-\infty}^{\infty} \int_{0}^{b} \mathrm{Re}\left[J_z J_z^*\right] dy d\xi \tag{89}$$

the current density, $J_z(\xi, y, t)$ is calculated using

$$J_z(\xi, y, t) = \sigma[v_x B_y(\xi, y, t) - E_z(\xi, y, t)] \tag{90}$$

and $B_y(\xi, y, t)$ and $E_z(\xi, y, t)$ are derived in Section 5.

5. TIME DOMAIN SOLUTION

In order to determine the force as a function of time (52) needs to be inverse Laplace transformed. Following the approach given in [33, 34] the transmission function, (32), can be rearranged and algebraically manipulated to yield

$$T(\xi, y, s) = \frac{\left(\dfrac{2k\cos(2ky/b)}{b\xi^2 \sin(2k)} + \dfrac{\sin(2ky/b)}{\xi \sin(2k)}\right)}{\left(-\lambda k + \cot(k)\right)\left(\lambda k + \tan(k)\right)} \tag{91}$$

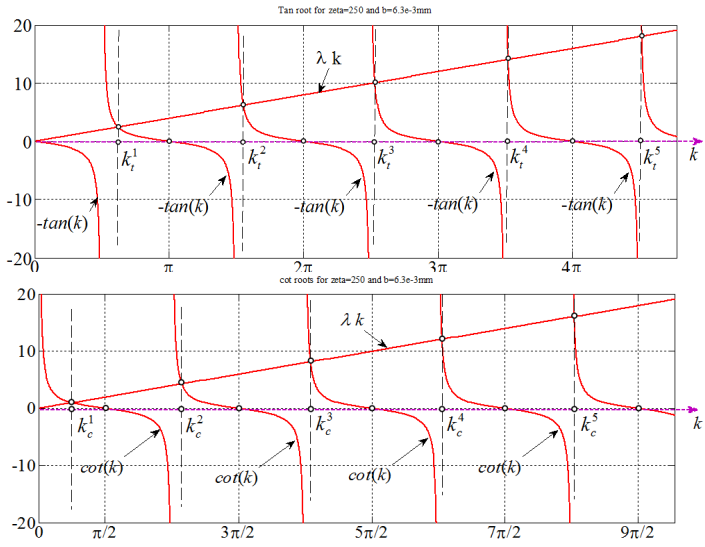

Figure 5. An example of the tan and cot roots calculation for $\xi = 250$ and $b = 6.3\,\text{mm}$.

where $\lambda = 2/\xi b$ and $k = -j\gamma b$ the advantage of using (91) rather than (32) is that the roots in the denominator can be easily determined [34]. They are given by

$$\tan(k) = -\lambda k \tag{92}$$

$$\cot(k) = \lambda k \tag{93}$$

The nth root of (92) is denoted by k_t^n and it lies between $n\pi + \pi/2$ and $n\pi + \pi$. The nth root of (93) denoted by k_c^n, lies between $n\pi$ and $n\pi + \pi/2$. An example plot of the roots of (92) and (93) for $\xi = 250$ and $b = 6.3\,\text{mm}$ is shown in Figure 5. The poles k_t^n and k_c^n both are purely located at negative values, and are given by

$$s_i^n = -\left[\left(\frac{2k_i^n}{b}\right)^2 + \xi^2\right]\frac{1}{\mu_o\sigma} \tag{94}$$

where the subscript $i = t$ or c. With the roots of (91) identified the expression for the field transmission coefficient for the nth root can be written as

$$T^k(\xi, y, k_i^n) = \frac{\left(\dfrac{2k_i^n\cos(2k_i^n y/b)}{b\xi^2\sin(2k_i^n)} + \dfrac{\sin(2k_i^n y/b)}{\xi\sin(2k_i^n)}\right)}{\left(-\lambda k_i^n + \cot(k_i^n)\right)\left(\lambda k_i^n + \tan(k_i^n)\right)} \tag{95}$$

The roots of (95) have been evaluated numerically by using the Heaviside expansion theorem [34, 35]. With the inverse of (95) determined the vector potential, (52), can be fully inverse transformed, this yields

$$A_z(\xi,y,t)=B^{s1}(\xi,b)T(\xi,y,s_1)e^{s_1t}+\sum_{m=0}^{9}\left[A_t^n(\xi,y)e^{s_t^nt}+A_c^n(\xi,y)e^{s_c^nt}\right] \quad (96)$$

where, s_t^n and s_c^n are given by (94) and

$$A_t^n(\xi,y) = -\frac{8k_t^n}{\mu_0\sigma b^2}\frac{\left(\dfrac{2k_t^n\cos(2k_t^ny/b)}{b\xi^2\sin(2k_t^n)}+\dfrac{\sin(2k_t^ny/b)}{\xi\sin(2k_t^n)}\right)}{(\cot(k_t^n)-\lambda k_t^n)(\lambda+\sec^2(k_t^n))} \left(\frac{B^{s1}}{(s_t^n-s_1)}-\frac{B^{s0}}{(s_t^n-s_0)}\right) \quad (97)$$

$$A_c^n(\xi,y) = \frac{8k_c^n}{\mu_0\sigma b^2}\frac{\left(\dfrac{2k_c^n\cos(2k_c^ny/b)}{b\xi^2\sin(2k_c^n)}+\dfrac{\sin(2k_c^ny/b)}{\xi\sin(2k_c^n)}\right)}{(\cot(k_c^n)-\lambda k_c^n)(\lambda+\sec^2(k_c^n))} \left(\frac{B^{s1}}{(s_t^n-s_1)}-\frac{B^{s0}}{(s_t^n-s_0)}\right) \quad (98)$$

This is the transient solution of the vector potential for a step change in the translational velocity from v_{x0} to v_{x1} and/or a step change in the electrical angular frequency from ω_{e0} to ω_{e1}. The change in airgap between the source and the conductive plate is also accounted for in (96). The first term is the steady-state solution of the vector potential at v_{x1} and ω_{e1} and the following two terms are the transient decaying response terms due to the step change.

The transient electric field intensity, E_z within the plate can also be obtained from A_z it is given by

$$E_z(\xi,y,t) = -\frac{dA_z(\xi,y,t)}{dt} = -s_1B^{s1}(\xi,b)T(\xi,y,s_1)e^{s_1t} - \sum_{m=0}^{9}\left(s_t^nA_t^n(\xi)e^{s_t^nt}+s_c^nA_c^n(\xi)e^{s_c^nt}\right) \quad (99)$$

and the magnetic flux density within the conductive region is given by

$$B_y(\xi,y,t) = -\frac{\partial A_z(\xi,y,t)}{\partial x} = -j\xi A_z(\xi,y,t) \quad (100)$$

$$B_x(\xi,y,t) = \frac{\partial A_z(\xi,y,t)}{\partial y} \quad (101)$$

The complete equation for the transient $B_x(\xi, y, t)$ field within the conductor can be obtained by substituting (96) into (101) as shown in [15].

6. VALIDATION USING FINITE ELEMENT ANALYSIS

The equations presented for this general analytic based model were compared with an FEA model capable of modeling both translational and rotational motion and a JMAG FEA model capable of modeling only rotational motion (Figure 6). The derivation of the FEA model formulation is presented in the appendix. The parameters used in

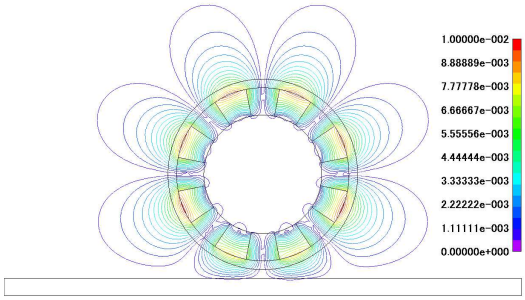

Figure 6. Vector potential fields for the transient JMAG model. The JMAG model could not model both rotational and translational motion of the rotor simultaneously. This model was used to verify the results shown in Figure 8.

Table 1. Simulation parameters.

Rotor	Outer radius, r_o	50 mm
	Inner radius, r_i	34.2 mm
	Magnet (NdFeB), B_r	1.42 T
	Magnet relative permeability, μr	1.055
	Pole-pairs, P	4
	Rotor width, w	50 mm
Conductive plate	Conductivity of aluminum plate, σ	2.459×10^7 Sm^{-1}
	Thickness, b	6.3 mm
	Air-gap between rotor and conducting plate, g	9.5 mm
	Conductive plate length, L	0.2 m

the comparison are given in Table 1. Figure 7 shows the comparison for the lift and thrust forces when $v_{x1} = 0\,\text{m/s}$ and a step change in angular velocity from 0 RPM to 3000 RPM occurs at time $t = 0\,\text{s}$; this is then followed by a second step change in velocity from 0 m/s to 10 m/s at 15 ms with angular velocity 3000 RPM. The reduction in lift and thrust force after 15 ms corresponds to the decrease in slip value. Figure 8 shows a force and power loss comparison for the case when $v_{x1} = 0\,\text{m/s}$ and a step change in angular speed from 0 to 3000 RPM occurs followed by a step change to 5000 RPM at $t = 15\,\text{ms}$. The airgap between the rotor and conductive plate is held constant in

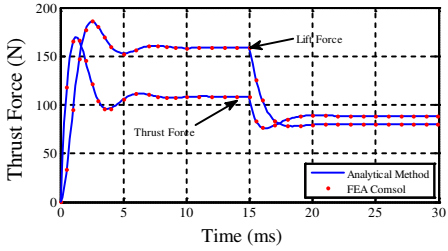

Figure 7. Transient lift and thrust force comparison for a step change in angular velocity from 0 RPM to 3000 RPM with velocity 0 m/s at $t = 0\,\text{ms}$ and a second step change of velocity from 0 m/s to 10 m/s at $t = 15\,\text{ms}$ with angular velocity = 3000 RPM.

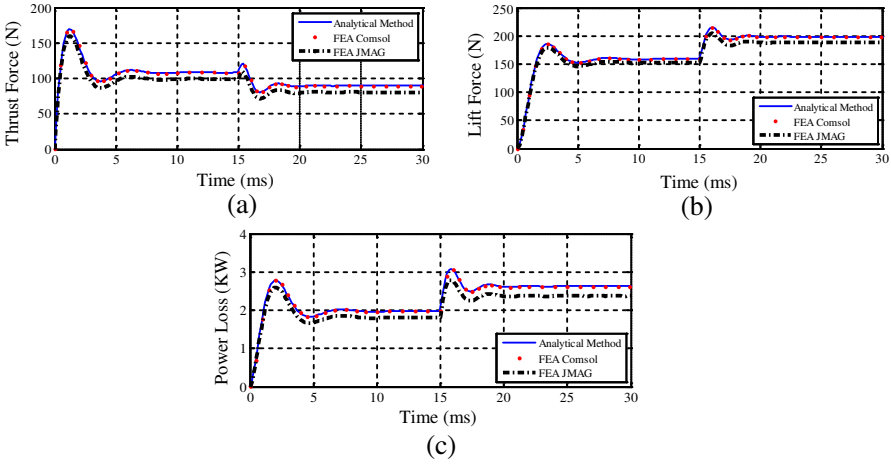

Figure 8. Transient results for (a) thrust force, (b) lift forces, (c) power loss for an RPM step change from 0 RPM to 3000 RPM at $t = 0\,\text{ms}$ and step change from 3000 RPM to 5000 RPM at $t = 15\,\text{ms}$, velocity = 0 m/s.

these simulations. The integral in (82) was evaluated using the Gauss-Kronrod quadrature numerical method from $\xi = 0$ to 250 (the source field is negligible for $\xi > 250$ and is zero for $\xi < 0$ due to the step function in (64)).

7. CONCLUSIONS

A general 2-D analytic based transient formulation for a magnetic source moving above a conductive plate has been derived. The formulation is written in a general form so that any magnetic source can be utilized. The derived field and force equations need to be computed by evaluating a single integral. The conductive region was solved for the vector potential whereas the air region was solved for the magnetic scalar potential. The inverse Laplace transform of the vector potential was obtained by using the Heaviside expansion theorem. The transient solution for the normal and tangential forces along the surface of the conductive plate were obtained by using Maxwell's stress tensor and Parseval's theorem. The use of Parseval's theorem circumvented the need for inverse Fourier transforming. The derived equations were validated by comparing them with two different 2-D FEA transient models.

APPENDIX A.

Assuming that the conductive plate is translationally moving with velocity, v_x (rather than the source field) then (1) will have a convective term present within the conductive plate such that

$$\frac{\partial^2 A_z}{\partial x^2} + \frac{\partial^2 A_z}{\partial y^2} = \mu_0 \sigma \frac{\partial A_z}{\partial t} + \mu_0 \sigma v_x \frac{\partial A_z}{\partial x} \tag{A1}$$

If the source in the non-conducting region is analytically modeled then the problem region will simplify down to a conducting region, Ω_2, and non-conducting regions, Ω_n ($n = 1, 3$) as shown in Figure 2. The boundary conditions given in (12)–(16) are also assumed to apply.

A.1. Conducting Plate Region, Ω_2

Using Galerkin weighted residual method and Green's identity (1) can be written in the weak form as [24]

$$\int_{\Omega_2} \nabla N_z \cdot \nabla A_z d\Omega_2 + \mu_0 \sigma \int_{\Omega_2} N_z \left(v_x \frac{\partial A_z}{\partial x} + \frac{\partial A_z}{\partial t} \right) d\Omega_2 - \int_{\Gamma_{12}} N_z (\nabla A_z \cdot \mathbf{n}_{c1}) d\Gamma_{12} - \int_{\Gamma_{23}} N_z (\nabla A_z \cdot \mathbf{n}_{c2}) d\Gamma_{23} = 0 \tag{A2}$$

where N_z is the shape function and $\mathbf{n}_{c1}$, $\mathbf{n}_{c2}$ are the unit outward normal vector on Γ_{12} and Γ_{23} respectively (refer Figure 2).

A.2. Non-conducting Regions, Ω_1, Ω_3

After using Green's first identity, the weak form of (5) in Ω_1 and Ω_3 are [24]

$$-\int_{\Omega_1} \nabla\phi_1 \cdot \nabla w_1 d\Omega_1 + \int_{\Gamma_{12}} w_1(\nabla\phi_1 \cdot \mathbf{n}_{nc1}) d\Gamma_{12} = 0 \tag{A3}$$

$$-\int_{\Omega_3} \nabla\phi_3 \cdot \nabla w_3 d\Omega_3 + \int_{\Gamma_{23}} w_3(\nabla\phi_3 \cdot \mathbf{n}_{nc3}) d\Gamma_{23} = 0 \tag{A4}$$

where w_1 and w_2 are the weighting function and $\mathbf{n}_{nc1}$, $\mathbf{n}_{nc2}$ are the unit outward normal vectors.

A.3. Boundary Conditions

The effect of the source field on the conductive region is accounted for by incorporated it into the interface between the conductive and non-conductive regions. The normal and tangential field components on the conductive boundary, Γ_{12} are given by

$$-\mu_0\nabla\phi_1 \cdot \mathbf{n}_{nc} + \mathbf{B}^s \cdot \mathbf{n}_{nc} = \nabla \times A_z \cdot \mathbf{n}_{nc}, \quad \text{on } \Gamma_c \tag{A5}$$

$$-\mathbf{n}_c \times \mu_0\nabla\phi + \mathbf{n}_c \times \mathbf{B}^s = \mathbf{n}_c \times \nabla \times A_z, \quad \text{on } \Gamma_c \tag{A6}$$

In order to couple conducting and non-conducting regions, the scalar boundary condition in (A3) needs to be expressed in terms of vector potential. Using (A5), the boundary term in (A3) can be written as

$$\int_{\Gamma_{12}} w_1\nabla\phi_1 \cdot \mathbf{n}_{nc} d\Gamma_{12} = \int_{\Gamma_{12}} \frac{w_1}{\mu_0}(\mathbf{B}^s - \nabla \times A_z) \cdot \mathbf{n}_{nc} d\Gamma_{12} \tag{A7}$$

Similarly the boundary condition in (A4) is replaced with [26]

$$\int_{\Gamma_{23}} w_3\nabla\phi_3 \cdot \mathbf{n}_{nc} d\Gamma_{23} = \int_{\Gamma_{23}} \frac{w_3}{\mu_0}(-\nabla \times A_z) \cdot \mathbf{n}_{nc} d\Gamma_{23} \tag{A8}$$

This then couples the scalar and vector equations together. The vector potential boundary conditions in (A2) must also be replaced with scalar terms. The boundary condition in (A2) in expanded form are

$$\int_{\Gamma_{12}} N_z \left[\frac{\partial A_z}{\partial x}\mathbf{n}_{c1x} + \frac{\partial A_z}{\partial y}\mathbf{n}_{c1y}\right] d\Gamma_{12} = 0 \tag{A9}$$

$$\int_{\Gamma_{23}} N_z \left[\frac{\partial A_z}{\partial x}\mathbf{n}_{c2x} + \frac{\partial A_z}{\partial y}\mathbf{n}_{c2y}\right] d\Gamma_{23} = 0 \tag{A10}$$

where $\mathbf{n}_{c1x}$ and $\mathbf{n}_{c1y}$ are the x and y normal vector components on the conductive boundary. Expanding (A5) enables (A9) and (A10) to be expressed in terms of scalar potential terms and source field as [26]

$$\int_{\Gamma_{12}} N_z \left[(\mu_0 \frac{\partial \phi_1}{\partial y} - B_y^s)\mathbf{n}_{cx} + (B_x^s - \mu_0 \frac{\partial \phi_1}{\partial x})\mathbf{n}_{cy} \right] d\Gamma_{12} = 0 \quad \text{(A11)}$$

$$\int_{\Gamma_{23}} N_z \left[(\mu_0 \frac{\partial \phi_1}{\partial y})\mathbf{n}_{cx} + (-\mu_0 \frac{\partial \phi_1}{\partial x})\mathbf{n}_{cy} \right] d\Gamma_{23} = 0 \quad \text{(A12)}$$

This then couples the scalar and vector formulations together within the conducting formulation. Similarly, the boundary condition in (A3) and (A4) are replaced with the vector potential terms (and source terms) such that [26]

$$\int_{\Gamma_{12}} w_1 \left(\frac{\partial \phi_1}{\partial x}\mathbf{n}_{nc1x} + \frac{\partial \phi_1}{\partial y}\mathbf{n}_{nc1y} \right) d\Gamma_{12}$$

$$= \int_{\Gamma_{12}} \frac{w_1}{\mu_0} \left(\left[B_x^{s1} - \frac{\partial A_z}{\partial y} \right] \mathbf{n}_{nc1x} + \left[B_y^{s1} + \frac{\partial A_z}{\partial x} \right] \mathbf{n}_{nc1y} \right) d\Gamma_{12} \quad \text{(A13)}$$

$$\int_{\Gamma_{23}} w_3 \left(\frac{\partial \phi_3}{\partial x}\mathbf{n}_{nc3x} + \frac{\partial \phi_3}{\partial y}\mathbf{n}_{nc3y} \right) d\Gamma_{23}$$

$$= \int_{\Gamma_{23}} -\frac{w_3}{\mu_0} \left(-\frac{\partial A_z}{\partial y}\mathbf{n}_{nc3x} - \frac{\partial A_z}{\partial x}\mathbf{n}_{nc3y} \right) d\Gamma_{23} \quad \text{(A14)}$$

Using (A2)–(A4) with the boundary condition coupling terms (A11)–(A14) as well as outer boundary conditions (12)–(16), enables the convective transient finite element **A**-ϕ model to be developed. A field plot created by this presented FEA model is illustrated in Figure A1.

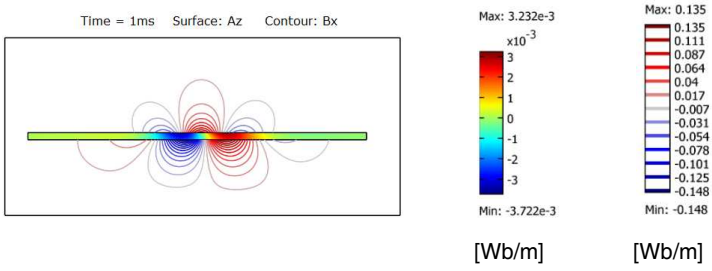

Figure A1. Contour and surface field plot for the 2-D FEA A_z-ϕ model (developed in COMSOL). With this formulation the Halbach rotor source is only present in the conducting boundary condition.

ACKNOWLEDGMENT

The authors would gratefully like to thank the JMAG Corporation for the use of their finite-element analysis software. This material is based upon work supported by the United States National Science Foundation under Grant No. 0925941.

REFERENCES

1. Mendrela, E. A. and E. Gierczak, "Two-dimensional analysis of linear induction motor using Fourier's series method," *Arch. Elektrotech.*, Vol. 65, Nos. 1–2, 97–106, Jan. 1982.
2. Lee, S. and R. C. Menendez, "Force on current coils moving over a conducting sheet with applications to magnetic levitation," *Proc. IEEE*, Vol. 62, No. 5, 567–577, May 1974.
3. Reitz, J. R. and L. C. Davis, "Force on a rectangular coil moving above a conducting slab," *J. Appl. Phys.*, Vol. 43, No. 4, 1547–1553, Apr. 1972.
4. Borcherts, R. H. and L. C. Davis, "Force on a coil moving over a conducting surface including edge and channel effects," *J. Appl. Phys.*, Vol. 43, No. 5, 2418–2427, May 1972.
5. Freeman, E. M. and C. Papageorgiou, "Spatial Fourier transforms: A new view of end effects in linear induction motors," *Proc. IEE*, Vol. 125, No. 8, 747–753, Aug. 1978.
6. Yamamura, S., *Theory of Linear Induction Motors*, University of Tokyo Press, 1979.
7. Panas, S. M. and E. E. Kriezis, "Determination of the field and the forces on a current filament moving above a conducting plate," *Arch. Elektrotech.*, Vol. 68, No. 4, 293–298, 1985.
8. Paudel, N. and J. Z. Bird, "General 2D steady-state force and power equations for a traveling time-varying magnetic source above a conductive plate " *IEEE Trans. Mag.*, Vol. 48, No. 1, 95–100, Jan. 2012.
9. Davis, L. C. and D. F. Wilkie, "Analysis of motion of magnetic levitation systems: Implications for high-speed vehicles," *J. Appl. Phy.*, Vol. 42, No. 12, 4779–4793, Nov. 1971.
10. Moon, F. C., *Superconducting Levitation*, John Wiley & Sons, New York, 1994.
11. Fink, H. J. and C. E. Hobrecht, "Instability of vehicles levitated by eddy current repulsion-case of an infinitely long current loop," *J. App. Phy.*, Vol. 42, No. 9, 3446–3450, Aug. 1971.

12. Krakowski, M., "Eddy currents in a metallic disk and axial force on it due to suddenly applied magnetic field," *Archiv fur Elektro.*, Vol. 65, Nos. 11–13, 1982.
13. Bird, J. and T. A. Lipo, "Calculating the forces created by an electrodynamic wheel using a 2D steady-state finite element model," *IEEE Trans. Mag.*, Vol. 44, No. 3, 365–372, Mar. 2008.
14. Langerholc, J., "Electrodynamics of a magnetic levitation coil," *J. App. Phy.*, Vol. 44, 2829–2837, 1973.
15. Paudel, N., "Dynamic suspension modeling of an eddy-current device: An applicaiton to MAGLEV," Ph.D. Thesis, Electrical and Computer Engineering, University of North Carolina at Charlotte, Charlotte, NC, 2012.
16. Faiz, J., "Time stepping finite element analysis of broken bars fault in a three-phase squirrel-cage induction motor," *Progress In Electromagnetic Research*, Vol. 68, 53–70, 2007.
17. Bedrosian, G., "High-performance computing for finite element methods in low-frequency electromagnetics," *Progress In Electromagnetic Research*, Vol. 7, 57–110, 1993.
18. Tsuboi, H., M. Tanaka, T. Misaki, and T. Naito, "Computation accuracies of boundary element method and finite element method in transient eddy current analysis," *IEEE Trans. Mag.*, Vol. 24, No. 6, 3174–3176, Nov. 1988.
19. Paudel, N., J. Z. Bird, S. Paul, and D. Bobba, "Modeling the dynamic suspension behavior of an eddy current device," *IEEE Energy Conv. Cong. Exp.*, 1692–1699, Phoenix, AZ, Sep. 17–22, 2011.
20. Lindell, I. V. and A. H. Sihvola, "Reflection and transmission of waves at the interface of perfect electromagnetic conductor," *Progress In Electromagnetic Research B*, Vol. 5, 169–183, 2008.
21. Sodano, H. A. and J. Bae, "Eddy current damping in structures," *Shock Vib. Dig.*, Vol. 36, 469–478, Nov. 2004.
22. Thompson, M. T., "Practical issues in the use of NdFeB permanent magnets in maglev, motors, bearings, and eddy current breaks," *Proc. IEEE*, Vol. 97, No. 11, 1758–1767, Nov. 2009.
23. Hellinger, R. and P. Mnich, "Linear motor-powered transportation: History, present status, and future outlook," *Proc. IEEE*, Vol. 97, No. 11, 1892–1900, Nov. 2009.
24. Bird, J. and T. A. Lipo, "Modeling the 3-D rotational and translational motion of a Halbach rotor above a split-sheet guideway," *IEEE Trans. Mag.*, Vol. 45, No. 9, 3233–3242, Sep. 2009.

25. Kirpo, M., S. Tympel, T. Boeck, D. Krasnov, and A. Thess, "Electromagnetic drag on a magnetic dipole near a translating conducting bar," *J. Appl. Phy.*, Vol. 109, No. 113921, 2011.
26. Williamson, S. and E. K. C. Chan, "Three-dimensional finite-element formulation for problems involving time-varying fields, relative motion, and magnetic saturation," *Proc. IEE Part A*, Vol. 140, No. 2, 121–130, Mar. 1993.
27. Xia, Z. P., Z. Q. Zhu, and D. Howe, "Analytical magnetic field analysis of Halbach magnetized permanent-magnet machines," *IEEE Trans. Mag.*, Vol. 40, No. 4, 1864–1872, 2004.
28. Atallah, K., D. Howe, P. H. Mellor, and D. A. Stone, "Rotor loss in permanent-magnet brushless AC machines," *IEEE Trans. Ind. Appl.*, Vol. 36, No. 6, 1612–1618, Nov./Dec. 2000.
29. Muramatsu, K., T. Nakata, N. Takahashi, and K. Fujiwara, "Comparison of coordinate systems for eddy current analysis in moving conductors," *IEEE Trans. Mag.*, Vol. 28, 1186–1189, 1992.
30. Polyanin, A. D. and A. V. Manzhirov, *Handbook of Mathematics for Engineers and Scientists*, Chapman & Hall, 2007.
31. Freeman, E. M. and C. Papageorgiou, "Spatial Fourier transforms: A new view of end effects in linear induction motors," *Proc. IEE*, Vol. 125, No. 8, 747–753, Aug. 1978.
32. Griffiths, D. J., *Introduction to Electrodynamics*, 3rd Edition, Prentice Hall, 1999.
33. Hannakam, L., "Transienter skineffekt in einer platte endlicher dicke bei beeliebiger form der erregenden leiterschleife," *Arch. Elektrotech.*, Vol. 60, 361–371, 1978.
34. Theodoulidis, T., "Developments in calculating the transient eddy-current response from a conductive plate," *IEEE Trans. Mag.*, Vol. 44, No. 7, 1894–1896, 2008.
35. Churchill, R. V., *Operational Mathematics*, 3rd Edition, McGraw-Hill, Inc., 1972.